Chapter 5

Auxetic Structures: Parametric Optimization, Additive Manufacturing, and Applications

Chapter details

Chapter DOI:

https://doi.org/10.4322/978-65-86503-83-8.c05

Chapter suggested citation / reference style:

Francisco, Matheus B., et al. (2022). “Auxetic Structures: Parametric Optimization, Additive Manufacturing, and Applications”. *In* Jorge, Ariosto B., et al. (Eds.) *Fundamental Concepts and Models for the Direct Problem,* Vol. II, UnB, Brasilia, DF, Brazil, pp. 120–153. Book series in Discrete Models, Inverse Methods, & Uncertainty Modeling in Structural Integrity.

P.S.: DOI may be included at the end of citation, for completeness.

Book details

Book: Fundamental Concepts and Models for the Direct Problem

Edited by: Jorge, Ariosto B., Anflor, Carla T. M., Gomes, Guilherme F., & Carneiro, Sergio H. S.

Volume II of Book Series in:

Discrete Models, Inverse Methods, & Uncertainty Modeling in Structural Integrity

Published by: UnB City: Brasilia, DF, Brazil Year: 2022

DOI: https://doi.org/10.4322/978-65-86503-83-8

Auxetic Structures: Parametric Optimization, Additive Manufacturing, and Applications

Matheus B. Francisco[1*], João L. J. Pereira[2], and Guilherme F. Gomes[3]

[1]Institute of Production Engineering and Management, Federal University of Itajubá, Brazil. E-mail: matheus_brendon@unifei.edu.br
[2]Institute of Mechanical Engineering, Federal University of Itajubá, Brazil. Email: joaoluizjp@gmail.com
[3]Institute of Mechanical Engineering, Federal University of Itajubá, Brazil. Email: guilhermefergom@unifei.edu.br

*Corresponding author

Abstract

This chapter focuses on presenting some concepts about auxetic structures. These models are known to have a negative Poisson's ratio, making them have some improved properties over conventional structures. The auxetics can be constructed with auxetic materials or conventional ones if they adopted the appropriate configuration to generate this behavior. Some configurations (reentrant, double arrowhead, chiral and rotated squares) will be presented in this work and will also be shown the manufacture via 3D printing of auxetic models. The additive manufacturing is a process widely used in the manufacture of auxetics. The application and the optimization of some of these structures will be related. It is expected that at the end of the chapter, the reader will be familiar with auxetic structures.

Keywords: Auxetic Structures; Poisson's ratio; Optimization; Additive Manufacturing; Surrogate Modeling; Design of Experiments.

1 An Overview of Auxetic Structures

The relationship between transversal and longitudinal strain is given by Poisson's ratio. This property is influenced by the atomic density of the materials, that is, the denser the atomic density, the higher its Poisson's ratio tends to be. For example, the Poisson's ratio of gold is higher than that of steel. Furthermore, analyzing some crystalline structures such as centered cubic face (CCF), hexagonal closed packed (HCP), body centered cubic (BCC) and diamond cubic (DC) it is possible to notice that the structures with higher atomic density also have higher Poisson's ratio, i.e. $\nu_{fcc} > \nu_{hcp} > \nu_{bcc} > \nu_{dc}$.

The materials or structures that presents negative Poisson's ratio (NPR) are known as auxetics, that is, they expand in the transverse direction when are pulled in the vertical direction. This behavior is different from conventional materials (steel, carbon, rubber, wood) that have to compress in the transverse direction during a longitudinal tensile load to compensate the loss of density. The discovery of auxetic behavior in some materials caused several research to be done seeking to understand its properties, and many things were discovered. However, much research still needs to be done today.

Most of the auxetic materials shown in literature are polymeric, which makes these materials less resistant to mechanical stresses. One way around this problem is to construct structures with conventional materials so that it has auxetic behavior. This is possible because of the configuration in which the structure is constructed, using some unit cells that provide the negative Poisson's ratio, such as: reentrant, double-V, perforated models. Each of these models has its advantages and disadvantages and the choice by one of them is depending on the application of the structure, the tools available for manufacture, the material to be used and so on.

It is also possible to construct composite auxetics using the joining of auxetics and non-auxetics materials for the development of the structure. The great advantage of this technique is to be able to join the properties of two (or more) different materials to arrive at better properties of the model. The research found in literature using these multi-material auxetics can be divided into 4 groups: modification of the lamination angle; produce auxetic structures using auxetic matrix; explore and evaluating the properties of these structures and design and build auxetics composites.

The auxetic models has better performance than conventional ones in several applications, such as more efficient and resistant filters [Quisse et al., 2016], special prosthetic materials [Vinay et al., 2019], improved protective equipment [Duncan et al., 2018] and medical implants of expandable stents [Gat et al., 2015]. The high energy absorption and fracture resistance of the auxetics makes them suitable for defense applications, for example, body armour [Linforth et al., 2020], shock-absorbing equipment [Duncan et al., 2016] and packaging materials [Tomazinziz et al., 2019]. Other's properties of auxetic are the increased shear modulus and indentation resistance [Evans et al., 2000], higher energy absorption capabilities [Scarpa et al., 2003], and better fracture toughness [Lakes and Elms., 1993]. The applications of this type of structure are diverse and many studies have been carried out in recent years covering several areas such as aerospace [Lira et al., 2011] and medical: smart bandages [White, 2009], dilators [Evan et al., 2000], antenna [Gupta and Gupta, 2005], and protective pads [Yang et al., 2016].

Figure 1a shows the application of auxetics in ballistic/fragment impacts [imbalzano et al., 2017]. Military cars are subject to passing through uneven terrain and with fragments of war products. In this way, these cars are subject to various impacts on the bottom and the use of auxetics to absorb energy from these impacts can protect the car and the people who are driving. Figure 1b shows the use of auxetics within a wing profile [Wu et al., 2019]. This can be used to absorb energy and control the level of vibration, for example. Finally, Figure 1c shows a medical application of auxetics [Mir et al., 2014]. It is known that the vascular system of the body shows anisotropic behavior, whereas the conventional coronary stents have isotropic properties. This results in a mismatch between anisotropic-isotropic properties of the stent and arterial wall, and this in turn is not favorable for mechanical adhesion of the conventional coronary stents with the arterial wall. It is believed that an auxetic coronary stent with inherent anisotropic mechanical properties and negative Poisson's ratio will have good mechanical adhesion with the arterial wall.

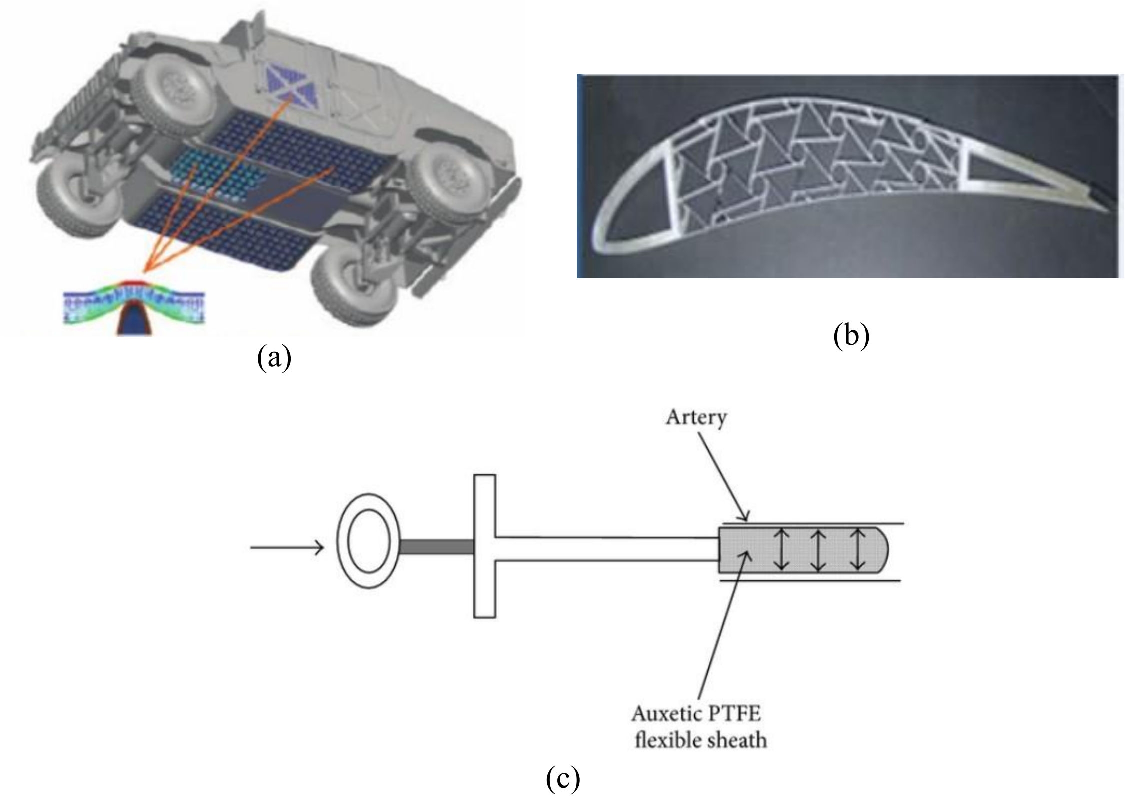

Figure 1: Auxetic application in (a) fragment impact protection [Imbalzano et al., 2017], (b) energy absorption in a wing [Wu et al., 2019] and (c) medical stent [Mir et al., 2014].

1.1 Poisson's ratio in the Mechanic of Materials

The relationship between longitudinal and transverse strain is given by Poisson's ratio (Equation 1). In conventional structures, the deformations have contrary signs, obtaining the positive Poisson's ratio. In auxetics, the strain has the same signal generating NPR.

$$\nu = -\frac{\varepsilon_x}{\varepsilon_z} = -\frac{\varepsilon_y}{\varepsilon_z} \tag{1}$$

where ν is the Poisson's ratio, ε_x, ε_y and ε_z are the strains in the x, y, and z direction, respectively. This property influence on the behavior of the structures and several studies were done to understand the points of improvement and the points of worsening in the model. For example, Guo et al. [2020] studied the deformation behaviors and energy absorption of auxetic lattice cylindrical structures under axial crushing load. The author compared auxetic cylindrical structures with conventional cylindrical structures to analyze which one had the best performance, concluding that the structures with negative Poisson's ratio had better performance.

The Poisson's ratio of isotropic materials depends of the modulus of elasticity (E), the shear modulation (G) and the bulk modulus (K), as shown in Equation 2 and 3. Combining the Equation 2 and 3, it is possible to find the Equation 4 that represent the relation between G and K. Notice how the Poisson's ratio influences these properties and, consequently, the mechanical performance of these structures. Thus, the study of auxetics is of great importance to the scientific community. It is important to note that for anisotropic materials it is necessary to specify several elastic constants depending on the structural characteristics of the crystal.

$$\mathrm{G} = \frac{E}{2(1+\nu)} \tag{2}$$

$$\mathrm{K} = \frac{E}{3(1-2\nu)} \tag{3}$$

$$\frac{2G}{3K} = \frac{1-2\nu}{1+\nu} \tag{4}$$

In most known materials, bulk modulus (K) is larger than shear modulus (G). Thus, one can make the implication presented in Equation 5. Moreover, a necessary condition to obtain the NPR is that the shear modulus is larger than the buckling modulus, both of which must be positive. For the G in Equation 2 to be positive, we have that the Poisson's ratio must be greater than -1 and for K to be positive in Equation 3, the Poisson's ratio must be less than 0.5. Thus, the Poisson's ratio varies within this interval and the graph in Figure 2 can be constructed to show the restriction impost in Equation 5.

$$\frac{2}{3} \leq \frac{1-2\nu}{1+\nu} \tag{5}$$

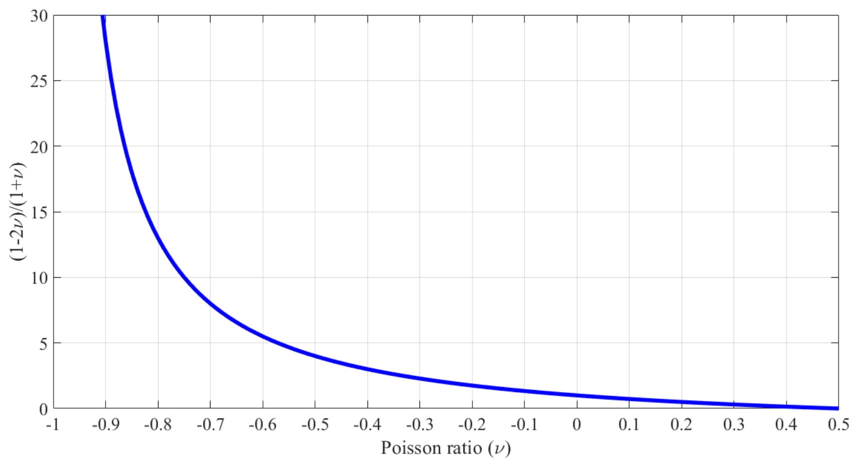

Figure 2: graphical relationship between ν and $\frac{1-2\nu}{1+\nu}$. [Francisco et al., 2021]

The Figure 2 shows that the Poisson's ratio gets smaller and smaller when the $\frac{2G}{3K}$ ratio increases. This ratio tends to infinity when the Poisson's ratio is trending to -1, on the other hand, the Poisson's ratio restriction being less than 0.5 prevents the values G and K to be negative. It is important to remember that this relationship applies to auxetic materials. For auxetic structures, calculations depend on the configuration adopted and the material used. Going further, it is worth remembering that to construct auxetic structures, it can be used auxetic or conventional materials, provided that the correct configuration for the construction of the model is adopted. The focus of this chapter is not to demonstrate the formulas for calculating the Poisson's ratio, but it is important to make it clear that the isotropic or anisotropic behavior of the material has a great influence on this parameter.

1.2 Natural and non-natural auxetic materials and structures

Materials with negative Poisson's ratio can be metallic [Ren et al., 2016], Ceramic [Hu et al., 2020], polymeric [Sahra and Dhanasekar, 2017], composite [Li et al., 2020]. Some examples of natural auxetic material are like α-cristoblaite [Evans et al., 1991], pyrolytic graphite [Voigt et al., 1966], some biological tissues [Lees et al., 1991] and crystalline cellulose [Yao et al., 2016], in a defined form, and α-quartz. While some materials have natural auxetic characteristics, others need to be modified to achieve these characteristics. Foam's materials, for example, exhibit conventional behavior, however, it is possible to obtain auxetic behavior by processing the material in the correct way [Najarian et al., 2018].

Auxetics foams are constructed from the compression of a piece of foam in all three directions and are subjected to temperature above the softening point of the material. After this process, they are removed and cooled to ambient temperature until they are removed from the mold. For polyester foams, Lakes and Roderic [1987] reported that a compression factor between 1.4 and 4 is sufficient to generate auxetic behavior in the structure. On the other hand, for reticulated metal foams, it is not necessary to use high temperatures.

2 Types of Cellular Auxetic Structures

Structures with negative Poisson's ratio can be constructed with conventional materials since the adopted configuration is suitable to generate an auxetic behavior. Some of these settings, which are recognized in literature and have already been used in several articles published around the world, will be shown in this section. However, it is important to note that there are several other existing models.

Additive manufacturing is a great ally in the manufacture of auxetics structures, as these often have complex configurations to be manufactured by conventional processes. Meena and Singamneni [2021] used the 3D printing technique to develop a novel hybrid auxetic structures for improved in-plane mechanical properties. The authors reported that the manufacture of this new part by a process other than 3D printing would make the cost of manufacturing the company unfeasible its production.

Several models have been created over the years through diverse different methodologies, for example: rotational structures [Grima et al., 2016]. , topology optimization [Gao et al., 2019], and taking inspiration from nature [Ren et al., 2018]. Some of the most famous auxetics configurations are re-entrant hexagonal honeycombs

[Liu et al., 2016], double arrowhead honeycomb [Wang et al., 2018], chiral [Zhang et al., 2018]. When additive manufacturing is used to manufacture structures, the print parameters influence the properties of the models. In addition, the material used also has great influence, Johnston and Kazanci [2021] carried out an analysis to know how three different material configurations effect the responses of three different cellular geometries and proved that the material really has great impact structural responses.

2.1 Re-entrant models

Gibson et al. [1982] were the pioneers to study reentrant models, they studied analytically the mechanic properties of a reentrant structure and performed experimental tests to validate the result. The authors developed models representing the mechanical properties of the structure in terms of bending, elastic buckling, and plastic collapse. The reentrant hexagonal model studied is shown in Figure 3. The value of the θ angle that makes the structure to be considered conventional or auxetic, i.e., if θ value is positive, the structure is conventional if the value is negative, there is an auxetic structure.

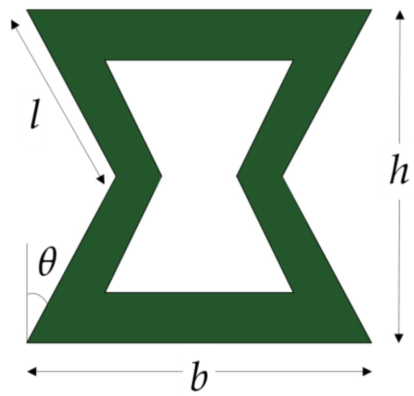

Figure 3: Design parameters of the reentrant auxetic unit cell.

Auxetic structures, in general, are periodic structures, that is, they have a unit cell that repeats itself throughout the model. Thus, you can analyze only one cell and extrapolate the results to the entire structure. Gibson et al. [1982] developed analytical models for the cell shown in Figure 3, the authors considered that each part of the cell can be considered a bar and that an external force caused a deformation in the structure. They found Equations 1 to 4 that describe, respectively, modulus of elasticity in the direction of force, modulus of elasticity in the direction transverse to force, Poisson's ratio and the shear modulus of the structure.

$$E_1 = \frac{K_f(\frac{b}{l} + sen\theta)}{hcos^3\theta} \tag{1}$$

$$E_2 = \frac{K_f cos\theta}{h\left(\frac{b}{l} + sen\theta\right) sen^2\theta} \tag{2}$$

$$\nu_{12} = \frac{sen\theta(\frac{b}{l} + sen\theta)}{cos^2\theta} \tag{3}$$

$$G_{12} = \frac{K_f(\frac{b}{l} + sen\theta)}{h\left(\frac{b}{l}\right)^2\left(1 + \frac{2b}{l}\right)cos\theta} \tag{4}$$

The ν_{21} can be found by the $E_1\nu_{21} = E_2\nu_{12}$ which is valid when one has the symmetric stiffness matrix. Two considerations were made by Gibson et al. [1982] during the development of the analytic models: bars deform only along their axis with no change in angle and the structure is under stretching efforts in vertical directions. the force exerted due to the applied stress σ_2 is given by Equation 5 and the P component of w that acts along the diagonal bar is given by Equation 6.

$$w = h\cdot(lsin\cdot\theta + b)\ cos\theta \tag{5}$$

$$P = h\cdot\sigma_2\cdot(l\cdot sin\theta + b)cos\theta \tag{6}$$

Knowing that the deformation of the structure is directly proportional to the applied force, we have that $P = K_s\delta$, where K_s is a tension constant. The deformation can be calculated by dividing equation 6 by tension constant, as shown in Equation 7, which, divided by length l, gives the strain given by Equation 8. Moreover, the relationship between the deformation, given by Equation 8, and the stress σ_2 is known as Hooke's law and is given by Equation 9.

$$\delta = \frac{h\sigma_2(lsen\theta + b)cos\theta}{K_s} \tag{7}$$

$$\varepsilon_2 = \frac{h\sigma_2(lsen\theta + b/l)cos\theta}{K_s} \tag{8}$$

$$E_2 = \frac{K_s}{h(lsen\theta + b/l)cos\theta} \tag{9}$$

Gibson et al. [1982] also made the calculations to find the deformation in direction 1, obtaining Equation 10. Thus, it is possible to find the Poisson's ratio by dividing the equation 8 by Equation 10. The Equation 11 shows the model for Poisson's ratio.

$$\varepsilon_1 = \frac{h\sigma_2 sen\theta cos\theta}{K_s} \tag{10}$$

$$\nu_{12} = -\frac{sen\theta}{sen\theta + \frac{b}{l}} \tag{11}$$

It is important to note that the Poisson's ratio of this model depends on the parameters θ, b and l. These three parameters are fundamental to define the auxetic behavior of the structure and, consequently, its mechanical properties.

2.2 Double-V models

Larsen et al. [1996] was one of the pioneers studying double arrowhead structures. Auxetic structures are periodic (repeat the same unit cell) and so the study of only one cell is sufficient to understand the behavior of the whole model. The parameters of a double-V cell is shown in Figure 4, It takes 3 cell parameters to build the model: two angles (θ_1 and θ_2) and the length l.

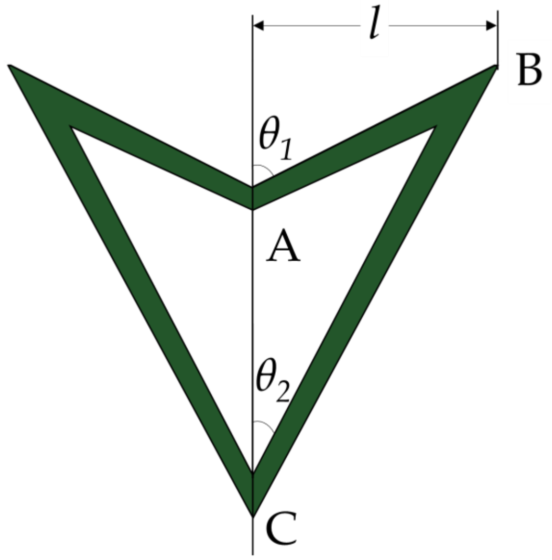

Figure 4: design parameter of the double arrowhead auxetic unit cell.

Qiao and Chen [2014] studied the double-V model analytically. The structure was subjected to a uniform stress σ_∞ which corrects a vertical force equal to $P_a = 2 \cdot \sigma_\infty \cdot lb \cdot$, where b is the dimension out of the plane of the structure. Some boundary conditions were adopted for the development of the analysis: the point C is constrained in all degrees of freedom and the point A is constrained to rotation and horizontal displacement (this implies in a reaction force F_a and reaction moment M_a when σ_∞ is applied). The Equation 12 and 13 shows the normal strains in x and y directions, when u_y^A is the vertical displacement of point A and u_x^B is the horizontal displacement of point B.

$$\varepsilon_y = \frac{u_y^A \cdot sin\theta_1 \cdot sin\theta_2}{l \cdot \sin(\theta_1 - \theta_2)} \tag{12}$$

$$\varepsilon_x = \frac{u_x^B}{l} \tag{13}$$

The relationship between equations 12 and 13 gives us the Poisson's ratio that is shown in Equation 14. It is also possible to calculate the modulation of elasticity, as shown in Equation 15 and 16, where E_s is the Young's modulus of the solid material and *I* is the second moment of inertia.

$$\nu_{xy} = -\frac{\varepsilon_x}{\varepsilon_y} = \frac{1}{tan\theta_1 \cdot tan\theta_2} \tag{14}$$

$$E_y = \frac{\sigma_\infty}{\varepsilon_y} = \frac{3E_sI}{bl^3}\alpha(\theta_1, \theta_2) \tag{15}$$

$$\alpha = -\frac{4(cos\theta_1 - cos\theta_2)}{sin\theta_1 sin\theta_2} - \frac{(cos\theta_1 cos\theta_2 - 1)^2(cos\theta_1 cos\theta_2 - 3)}{sin\theta_1 sin\theta_2(cos\theta_1 - cos\theta_2)} + \frac{(cos\theta_1 cos\theta_2 + 3)(cos\theta_1 cos\theta_2 - 1)}{cos\theta_1 - cos\theta_2} \tag{16}$$

It is noticed that θ_1 and θ_2 angles have influence on the Poisson's ratio value, the higher the angles, the lower the Poisson's ratio. This is because the angle interferes with the deformation capacity of the structure, that is, depending on the values of θ_1 and θ_2 , the structure will be able to deform more or less. Similarly, the angles also affect the modulation of elasticity, in addition, the length *l* also has influence.

2.3 Rotating squares and Rectangle models

Grima and Evans [2000] were the pioneers studying the rotating squares and rectangle models. The authors verified that this type of structure would have the Poisson's ratio equal to -1. In addition, they developed an analytic study to show the equations that govern the structure. The relationship between the deformation and the stress found by them is shown in Equation 17, being S the compliance matrix of the structure.

$$\begin{vmatrix} \varepsilon_1 \\ \varepsilon_2 \\ \gamma_{12} \end{vmatrix} = \begin{vmatrix} S_{11} & S_{12} & S_{13} \\ S_{21} & S_{22} & S_{23} \\ S_{31} & S_{32} & S_{33} \end{vmatrix} \bullet \begin{vmatrix} \sigma_1 \\ \sigma_2 \\ \tau_{12} \end{vmatrix} \tag{17}$$

$$S = \begin{vmatrix} \frac{1}{E_1} & \frac{-v_{21}}{E_2} & 0 \\ \frac{-v_{12}}{E_1} & \frac{1}{E_2} & 0 \\ 0 & 0 & 0 \end{vmatrix}$$

The authors also found the equation representing the young modulus of the structure and it is shown in Equation 18, where θ is the angle shown in Figure 5, *l* is the length of the squares and k_h is the rotational stiffness constant.

$$E_1 = E_2 = \frac{8k_h}{t^2(1 - sin\theta)} \tag{18}$$

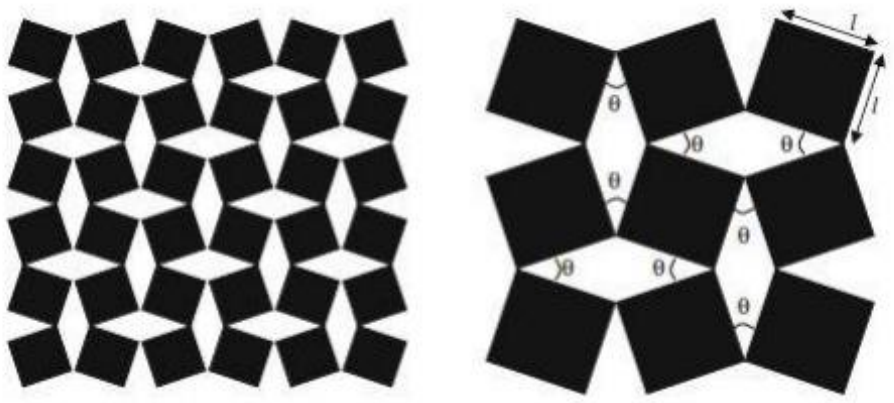

Figure 5: Auxetic model proposed by Grima and Evans: overview and details. [Grima and Evans, 2000]

Grima et al. [2007] continued studies in rotating squares to assess whether semi-rigid structures would also have an auxetic behavior. The authors developed an analytic study based on the model shown in Figure 6. Equations 19-39 shows the behavior of the model.

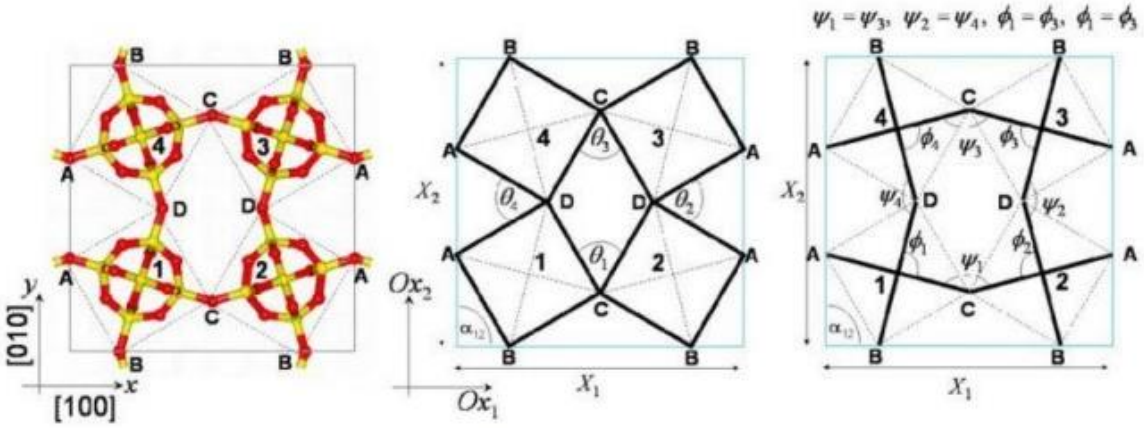

Figure 6: Variables used in the model proposed by Grima et al. [2007]

$$\nu_{12} = \nu_{21} = -cotg(\frac{\Psi_1}{2})tan(\frac{\Psi_2}{2})[\,1 + 4(\frac{K_\Psi}{K_\emptyset})]^{-1} \tag{19}$$

$$E_1 = E_2 = \frac{8K_\Psi(K_\emptyset + 2K_\Psi)}{l_d^2 z(K_\emptyset + 4K_\Psi)} \cdot \frac{sin(\frac{\Psi_2}{2})}{sin(\frac{\Psi_1}{2})cos^2(\frac{\Psi_2}{2})} \tag{20}$$

$$G_{12} = K_{\emptyset} \frac{1}{z} [l_d \, sin \, (\frac{\Psi}{2})]^{-2} \tag{21}$$

where l_d is the length of AC or BD (diagonal of the square) in figure 6, the rotational stiffnesis given by K_{φ} and $K_{\emptyset}$ that restrain changes to the angles φ and ∅, respectively, and z is the thickness in the third direction of the squares. Thus, it is possible to calculate the Poisson's ratio, the modulus of elasticity and the shear modulation by the following equations:

$$\nu_{12} = \nu_{21} = -[1 + 4(\frac{K_{\Psi}}{K_{\emptyset}})]^{-1} \tag{22}$$

$$E_1 = E_2 = \frac{8K_{\Psi}(K_{\emptyset} + 2K_{\Psi})}{l_d^2 z(K_{\emptyset} + 4K_{\Psi})} \cdot \sec^2 (\frac{\Psi}{2}) \tag{23}$$

$$G_{12} = \frac{K_{\emptyset}}{z l_d^2} [sin^2 \, (\frac{\Psi}{2})]^{-1} \tag{24}$$

The off axis elastic moduli at an angle ζ around the third direction are given by Grima et al. [2007] by Equation 25, 26 and 27. where m = cos(ζ) and n = sin(ζ).

$$\frac{1}{E_1^{\zeta}} = \frac{m^4}{E_1} + \frac{n^4}{E_2} - m^2n^2 \, (2 \cdot \frac{\nu_{12}}{E_1} - \frac{1}{G_{12}}) \tag{25}$$

$$\nu_{12}^{\zeta} = E_1^{\zeta} \, [(m^4 + n^4) \frac{\nu_{12}}{E_1} - m^2n^2(\frac{1}{E_1} + \frac{1}{E_2} - \frac{1}{G_{12}}) \tag{26}$$

$$\frac{1}{G_{12}^{\zeta}} = \frac{m^4 + n^4}{G_{12}} + 2m^2n^2 \, (\frac{2}{E_1} + \frac{2}{E_2} + \frac{1}{G_{12}} + \frac{4\nu_{12}}{E_1}) \tag{27}$$

2.4 Chiral Models

It is said that an object is chiral when there is no possibility of it to be superimposed on its mirrors image. The chiral models rotate when they receive compressive force, causing auxetic behavior to be evidenced. The movement of this type of structure while receiving a load is like what happens with transmissions and crankshaft [Necemer et al., 2020]. Prall and Lakes [1997] studied this type of structure through analytical and experimental analyses for strain in plane. The equations found by then that represent the deformations of the structure are shown in equations 28-30. Furthermore, the parameters used by the authors are shown in Figure 7.

$$e = r \cdot \sin\varphi \tag{28}$$

$$e_1 = r \cdot \varphi \cdot cos\theta \tag{29}$$

$$e_2 = r \cdot \varphi \cdot sin\theta \tag{30}$$

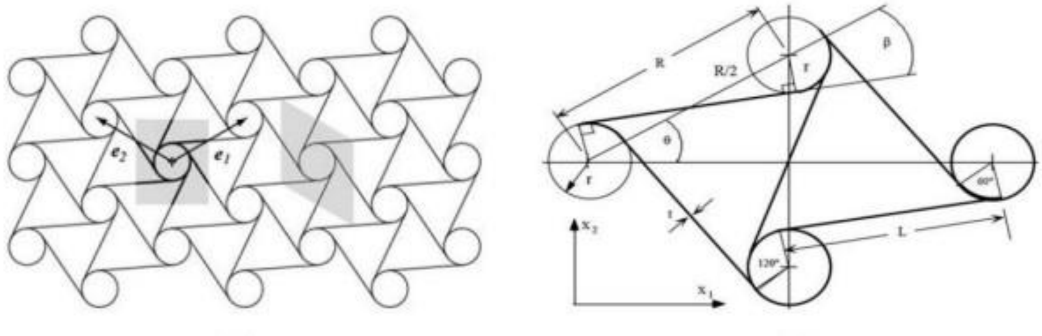

Figure 7: Geometry of a hexagonal chiral lattice. [Prall and Lakes, 1997]

where φ is the angle of applied deformation in the structure. The r·sinφ ~ r·φ can be made because the structure is subjected to small deformations. The Equation 31 shows the calculus of φ by the elementary beam theory, where *t* is the thickness of the structure, *d* is the width of the structure, E is the material Young's modulus and T is the applied load in the system.

$$\varphi = \frac{2LT}{Et^3d} \tag{31}$$

The authors concluded that the deformations ε_1 and ε_2 can be given by Equations 32 and 33, respectively. Furthermore, the Poisson's ratio is given by the relationship between the longitudinal and transversal deformed, as shown in Equations 34 and 35.

$$\varepsilon_1 = \varphi \cdot \frac{r}{R} \tag{32}$$

$$\varepsilon_2 = \varphi \cdot \frac{r}{R} \tag{33}$$

$$\nu_{12} = -\frac{\varepsilon_2}{\varepsilon_1} \tag{34}$$

$$\nu_{21} = -\frac{\varepsilon_1}{\varepsilon_2} \tag{35}$$

3 Auxetic Structures in Engineering

This section will be responsible for showing how auxetics structures are used within engineering. For this, it will be shown a way of manufacturing some models and then will be reported on some utilizations of this type of structure. It is important to note that there are several auxetic models and various applications of these models, it is not possible to exemplify all the possibilities here and only a few will be shown next.

3.1 Fabrication of auxetic models

Auxetic structures usually have a complex shape, which makes it difficult to manufacture. However, the advancement of additive manufacturing has greatly facilitated the development of these structures and has been widely used by many authors around the world. The author of this chapter manufactured three auxetic structures, using 3D printing, to exemplify the construction of these models. The structures that will be shown here were manufactured via 3D printing on the Ultimaker® 2+ printer using Polylactic acid (PLA) filament with a diameter of 1.75mm. The printing temperature and the build plate temperature is equal to 200°C and 60C°, respectively. The print speed, the layer height and the infill density are equal to 55mm/s, 0.4mm and 20%, respectively. Several materials can be used for manufacturing, however, in this section, polylactic acid (PLA) was used which is a polymer widely used for the manufacture of these models .

For the example of this section, it was used the auxetic model shown in figure 3 and 4, respectively. In addition, three auxetics structures were constructed: reentrant tube, reentrant beam, and double-V beam. The initial values of the design parameter for the reentrant beam are equal to 16mm, 8mm and 60° for the base length, oblique length and angle of the unit cell, respectively. Thus, the author adopted seven cells in the horizontal, three in the vertical direction and 30mm of death. The same parameters of the unit cell were used to construct the reentrant tube, the other parameters of the tube are shown in table 1.

Table 1: Design parameter adopted for the tube manufacturing.

Variable	Symbol	Unit	Value
Angle	α	degrees	60
Oblique length	l	mm	8
Horizontal length	b	mm	16
Height of Tube	H	mm	83.2
Diameter of Tube	D	mm	91.68
Height of Cell Unit	h	mm	13.85
N° of horizontal cell	N_c	-	24
N° of vertical cell	N_h	-	6

For the double-V model, the design parameters are shown in Figure 4 (angle θ_1 , angle θ_2 , and oblique length l). The values adopted to build the structure are θ_1 equal to 60°, θ_2 equal to 30° and oblique length l equal to 30mm. Thus, it will be adopted three cells in horizontal and four in vertical direction. All the models were designed in a software CAD and transferred to the Ultimaker Cura to set the print paramenters. Figure 8 shows the manufacturing process of the three models constructed and the final structure.

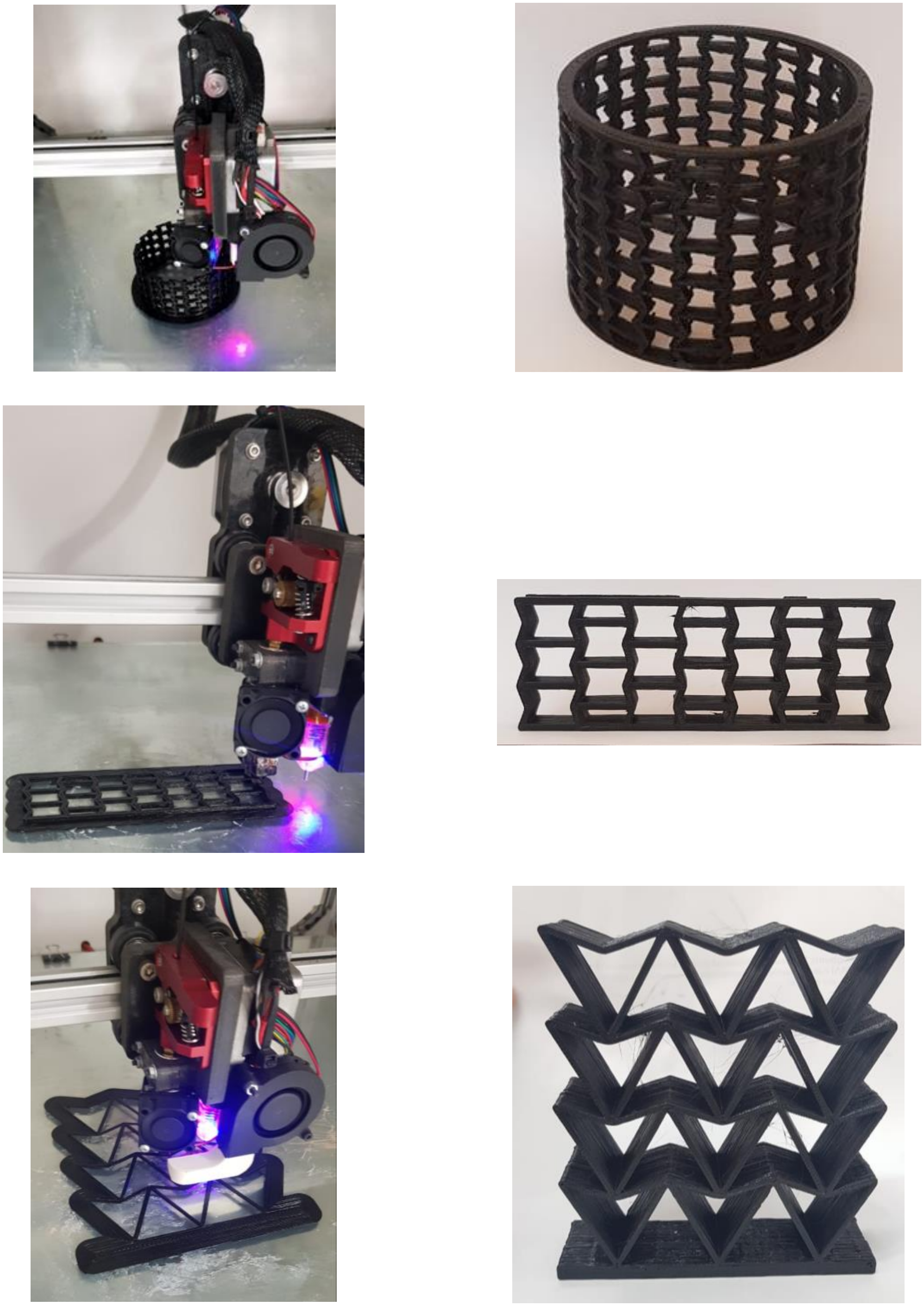

Figure 8: Manufacturing process and the final structures studied in this chapter.

3.1.1 Experimental Results of Auxetic Structures

The three structures proposed in this chapter were subjected to a compression test. Figure 9 shows the compression test carried out on the auxetic tube from the initial experiment (t=0s) until the end time (t = 140s). The maximum load reached was 3254 N and the mass of the structure is equal to 84.3g. Figure 10 shows the deformation of the part during the experimental test for the reentrant beam, the maximum load obtained by the structure was 12467N and has a mass of 70g. Finally, Figure 11 shows the deformation of the double-V structure during the compression test, the maximum load reached was 2100N and the mass of the structure was 116g. The table 2 compiles these results.

Table 2: Experimental results of the auxetic structures studied in this chapter.

Structure	Maximum load (N)	Mass (g)	Load-mass ratio (N/g)
Reentrant tube	3254	84.3	38.6
Reentrant beam	12467	70	178.1
Double-V beam	2100	116	18.1

Table 2 shows that the reentrant beam is the structure that gets the major maximum load and is the lightest structure of the three studied. However, the choice for one of them depends on the application and manufacturing process available. Furthermore, further tests should be performed to evaluate other responses together with the maximum compression load supported. It is important to note that all these parts were manufactured using the same printing parameters and the same material.

(INTENTTIONALY LEFT BLANK)

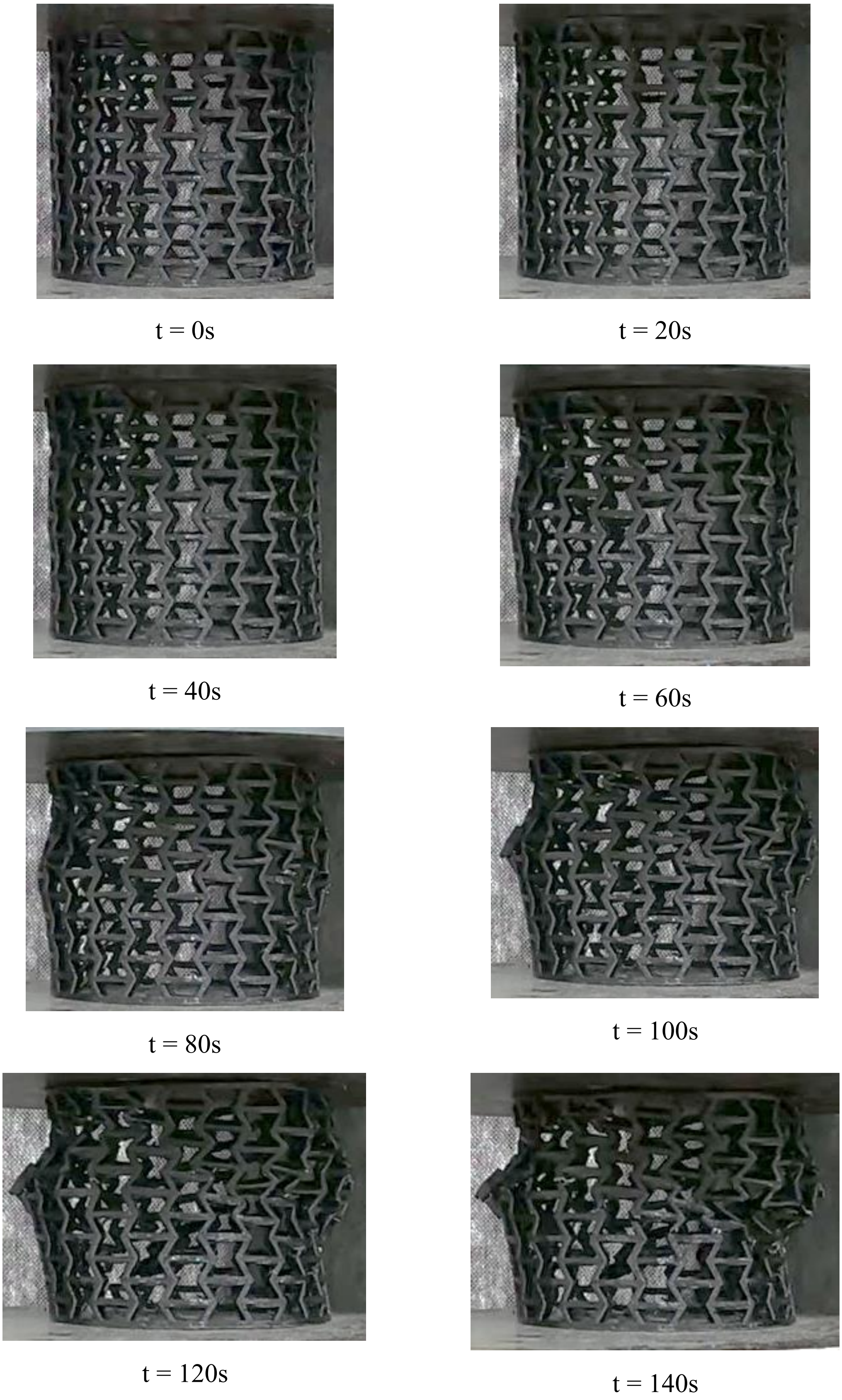

Figure 9: Performance of auxetic reentrant tube in compression tests.

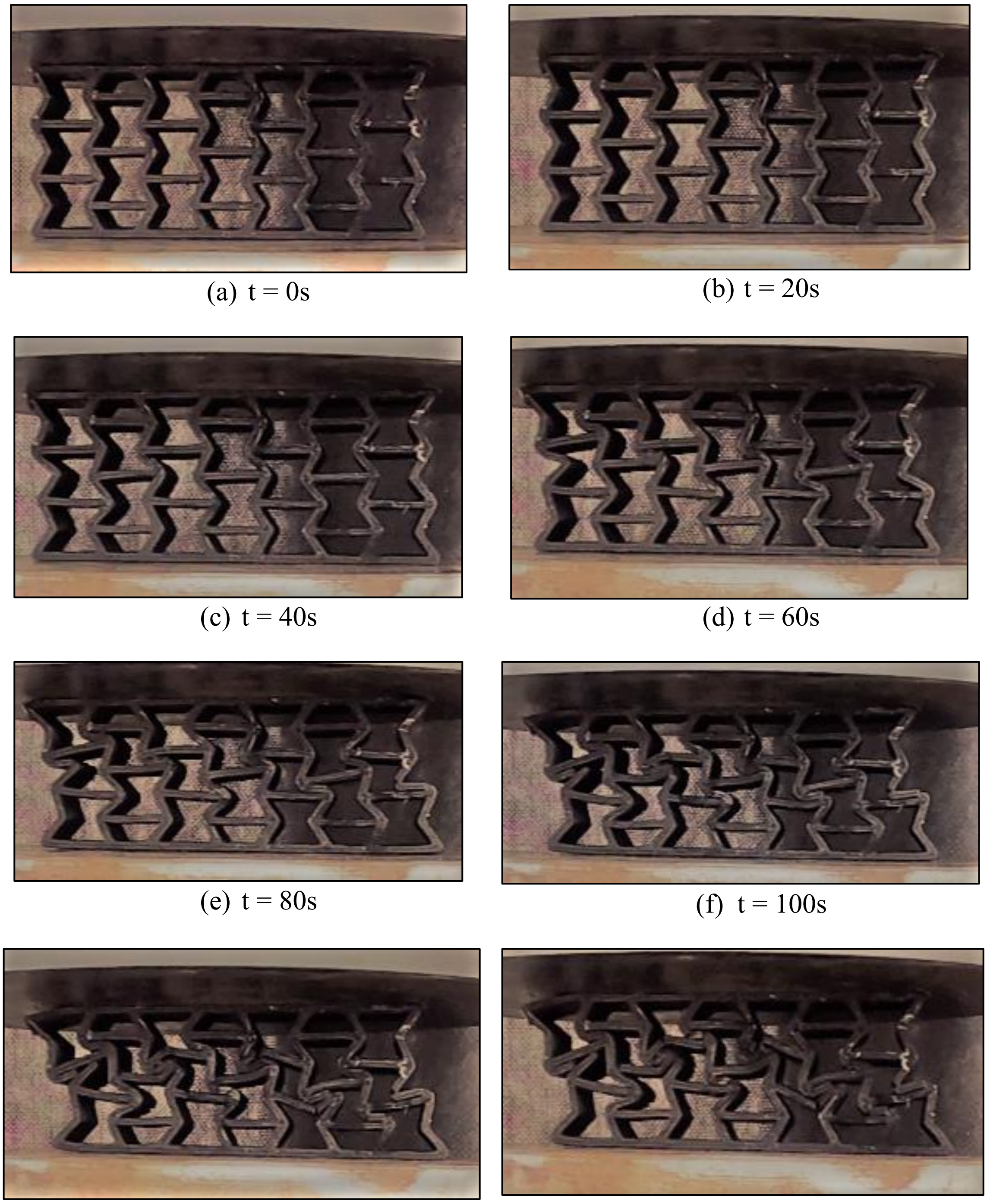

(a) t = 0s (b) t = 20s
(c) t = 40s (d) t = 60s
(e) t = 80s (f) t = 100s
(g) t = 120s (h) t = 140s

Figure 10: Performance of auxetic reentrant beam in compression tests.

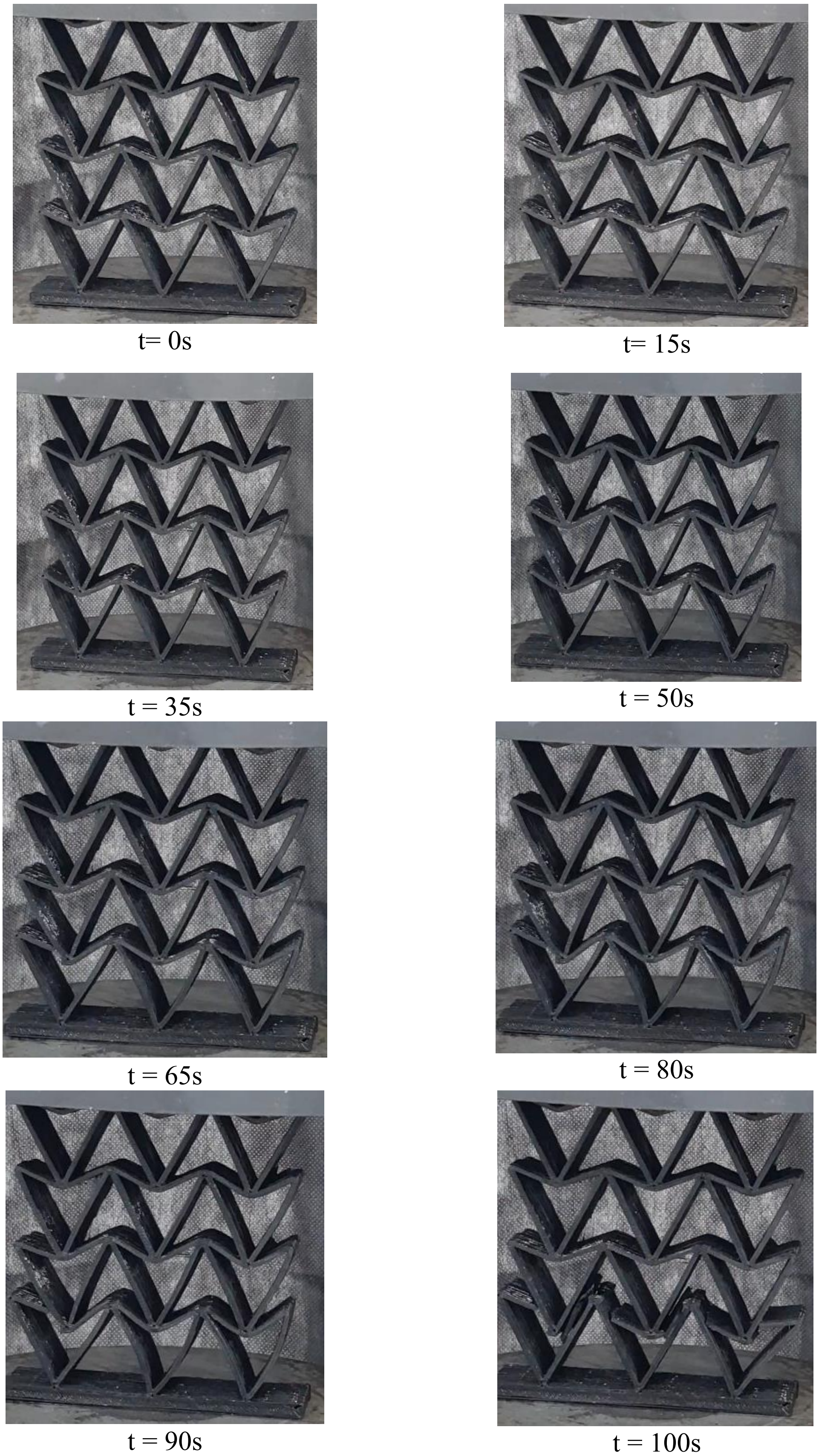

Figure 11: Performance of auxetic double-V beam in compression test.

3.2 Auxetic Structures Applied in Engineering

The idea of applying auxetics structures in engineering is not something recent, as it had its beginning around the 1970s. However, the difficulty of manufacturing these structures caused the studies not to prosper at that time. Today, additive manufacturing has been a great ally of the manufacture of auxetics structures, as it facilitated the manufacture of these models. Thus, several auxetics configurations began to appear and several applications for these models were studied, some of these applications will be shown in this section.

Foser et al. [2018] evaluated whether the use of auxetic foam in sport helmet was feasible. The author's objective was to study whether the use of this foam would improve its linear impact acceleration attenuation. Figure 12 shows the helmet used by the author. Furthermore, the author compared the results of the auxetics model with conventional ones, showing that auxetics have superior performance, i.e., Gadd severity index reduced by 11% for frontal impacts (39.9J) and 44% (24.3J) for side impacts. Thus, it was possible to verify that auxetics structures could be used for protection both in the sports industry and in other areas.

Shah et al. [2022] carried out a finite element analysis of the ballistic impact on auxetic sandwich composite human body armour. The authors analyzed with several different types of projections, comparing the responses of the auxetic structure with conventional structures. The author concluded that the indentation resistance improved with the auxetic armour and deformation in auxetic armor was observed greater for each of the cases when compared to the conventional armor, due to higher energy absorption. Thus, it is perceived that the investment in auxetics structures for protective equipment is valid and very important to improve the safety of current protective equipment.

Figure 12: Foam inserts: (a) foreheads, (b) right side and (c) left side [Shepherd et al., 2020].

The automotive industry is increasingly seeking to build light, comfortable and safe cars. The need for economical cars makes the reduction of their weight one of the main objectives in the design of automobiles. In addition, safety is also a very important item and the construction of a crash box (integral component for ensuring the safety of a car which serves as an energy absorbing member) should cause the car to absorb some of the energy in case of frontal collision during car accidents. Wang et al. [2018] analyze the application of auxetic structures to design jounce bumpers, this study was able to improve the noise, vibration, and harshness performance of the automobile. Zhou et al. [2016] carried out a multi objective optimization of an auxetic structure focused on building a crash box with auxetic structures and improving the collision performance of the car.

Other studies have also been done seeking to optimize the energy absorption of some components to increase car safety. Gao et al. [2018] studied a cylindrical auxetic structure in a novel crash box, compared with conventional models, the auxetic structure has lower peak crushing force and higher energy absorption. Lee et al. [2019] compared auxetic and conventional structures in development of a crash tube, and the performance of auxetic structures was superior to conventional structures. Thus, it can be noted that the use of auxetic structures in protective equipment is of great interest to the world scientific community.

Another much explored feature of auxetic structures is the damping mechanism. Chen et al. [2020] studied the damping mechanism of CFRP three-dimensional double-arrow-head auxetic structures. The author manufactured the structure in carbon fiber reinforced polymer (CFRP) and submitted it to compressive loading-unloading tests and sine sweep frequency experiments. The author compared the performance of the construction structure with a conventional structure, and the auxetics obtained better results, i.e., excellent comprehensive characteristics of light weight, high specific strength and high damping performance. The structure tested by the author is shown in Figure 13. This better damping capability makes these structures can be applied in conditions that need to reduce the vibration level or reduce vibration transmissibility.

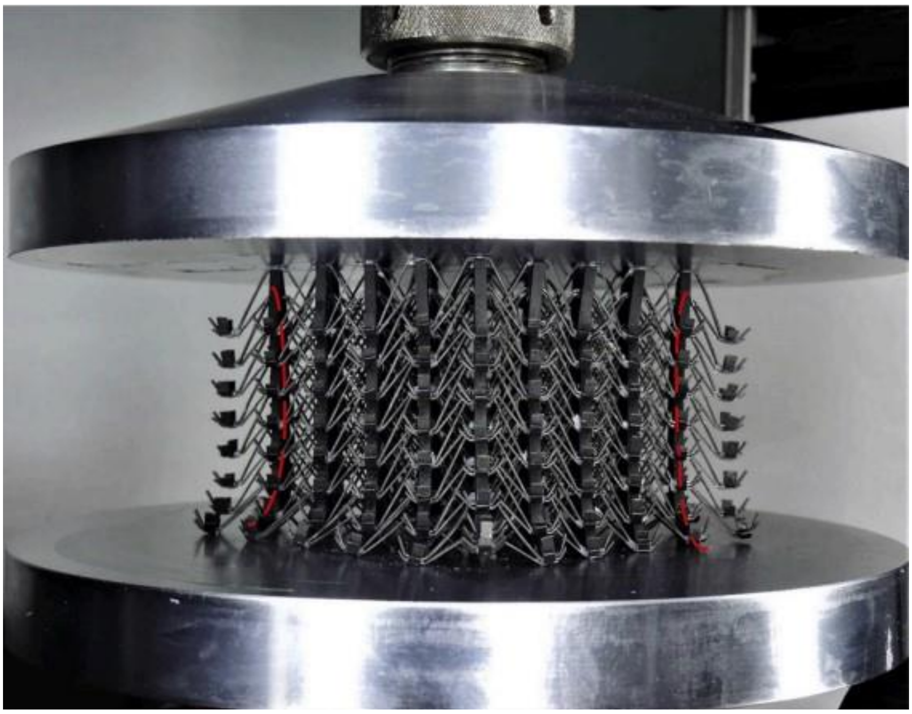

Figure 13: Deformed photograph of the 3D DAH structure during compression. [Chen et al., 2020]

Budarupu et al. [2016] studied the design concepts of an aircraft wing using morphing airfoil with auxetic structures. The authors evaluated the aerodynamic forces that appear on the flight during the flight to use as a contour condition. The advantages of the morphing airfoil with auxetic structure are (i) larger displacement with limited straining of the components and (ii) unique deformation characteristics, which produce a theoretical in-plane Poisson's ratio of – 1. The structure used by the author is shown in Figure 14. It is possible to notice that auxetics structures can be applied in various situations and that their use can generate several advantages over conventional structures.

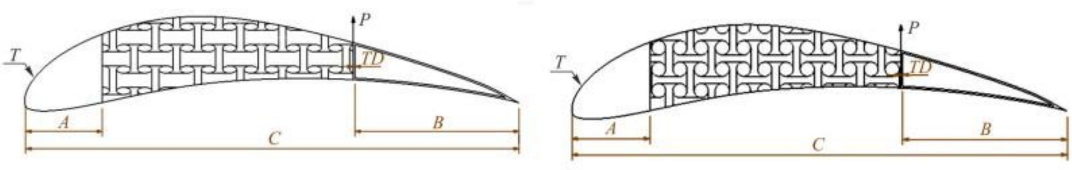

Figure 14: Airfoil with auxetic structure of (a) elliptical cells and (b) circular cells used by Budarupu et al. [2016].

Several other authors have published studies focused on the application of auxetic structures in real problems. Günaydin et al. [2019] used the anti-tetrachiral and reentrant models to study the deformation mechanism of these structures. The authors concluded that the auxetic models have higher performance in crush absorption than conventional ones thanks to its high shear strength, i.e., auxetics have better performance to be applied in automotive bumpers, for example. Figure 15a shows the application studied by Lee et al. [2019] He evaluated the performance of auxetic structures manufactured via additive manufacturing with SUS316L under low impact condition, concluding that these structures have better performance than conventional structures to absorb impact energy.

Figure 15b shows the model of the study conducted by Chang et al. [2017] which aimed to use auxetics structures to protect concrete structures against impact and blast loadings. The authors carried out two experimental tests: drop weight impact and filed blast test. The results showed that the plate made with auxetic structure absorbed 19.1% more energy than the plate built with conventional structures. This work showed the importance of the study of auxetic structures applied to protection systems. Figure 15c shows a new shock absorbing uniaxial graded auxetic damper developed by Al-Rifaie and Sumelka [2019]. The authors conducted several tests and found that this structure is applicable in various situations, such as: blast resistant doors; blast resistant for retrofitting sensitive buildings; elevator (absorbing unexpected crash of elevators or cable failure in multi-story buildings); crash energy absorbing system in motor vehicles front bumpers; and many other possible applications.

Finally, Figure 15d shows the fuselage sections with negative Poisson's ratio structure insert below the cargo floor studied by Wang et al. [2021]. The author studied the use of these structures in the aircraft fuselage to assess the energy absorption capacity during a crash landing. They concluded that these structures have better energy absorption performance than conventional structures and that they have potential in improving the crashworthiness behavior of aircraft.

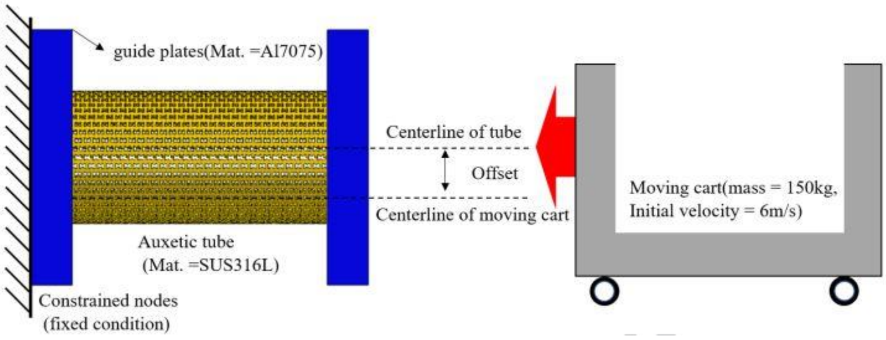

(a)

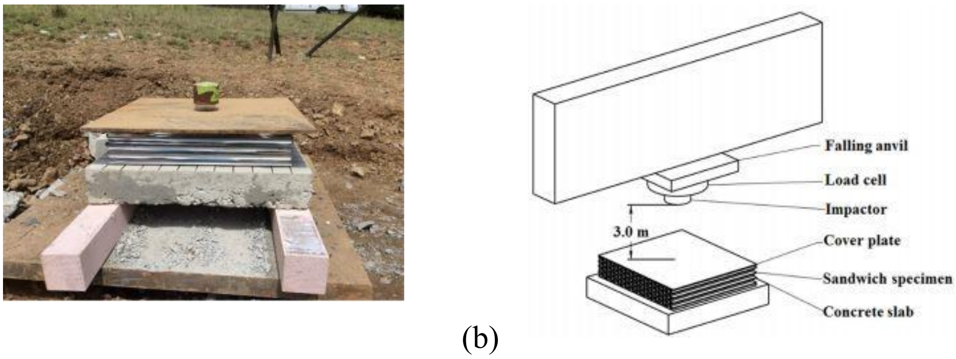

(b)

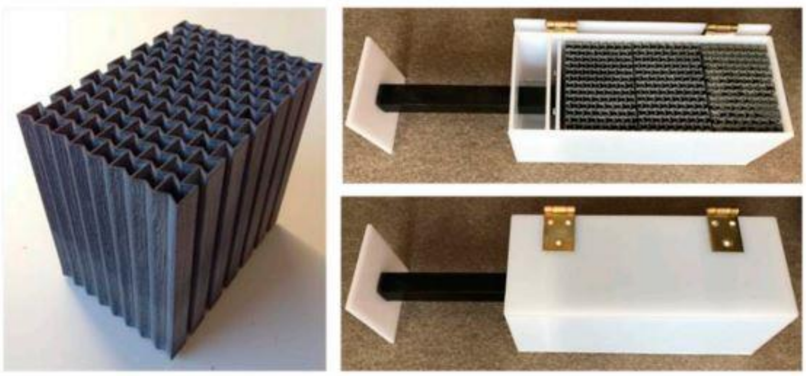

(c)

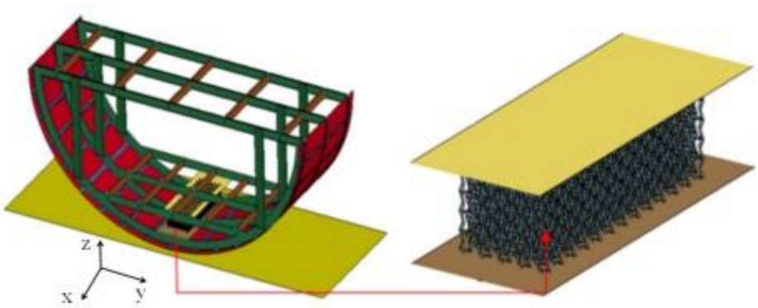

(d)

Figure 15: Examples of auxetic applications: (a) automotive bumpers [Lee et al., 2019] (b) protective systems against impact [Chang et al., 2017] (c) shock absorbing [Al-Rifaie and Sumelka, 2019] and (d) aircraft's fuselage [Wang et al., 2021].

4 Optimization of Auxetic Structures

Auxetic structures can be applied in various situations and the optimization of these models for each of the applications is very important. Optimization can be mono objective, when there is only one objective, or multi-objective when you want to optimize multiple responses simultaneously. This second methodology is more real, because the structures are subjected to several loads simultaneously during their operation. In this section, a methodology called parametric optimization will be shown.

4.1 Parametric optimization in Auxetic Structures

Parametric optimization is a methodology used to find the best design variables of a given structure. In this section, we will demonstrate a parametric optimization study of a reentrant beam. For this, we first need to figure out which variables are important to the problem, so that we will use them to get our goal. Thinking of a reentrant cell, equations 1-11 can be used to describe the structure analytically. Moreover, it is perceived by equation 11 that the Poisson's ratio of the structure depends on b (length of the horizontal bar), l (length of the oblique bar) and θ (angle between these bars).

From the moment we find which design variables are important for the analysis, it is necessary to find out in which range is the optimal point. This is a very difficult task and can be done in two ways: using the experience of the designer or doing an exploratory analysis. Generally, when the designer knows very well the behavior of the structure, he can deduce within what range the design parameters can stay to achieve good results. If you do not have this knowledge, exploratory analysis is the best option. Exploratory analysis consists of performing some experiments to find the intervals of the design parameters that best generate results.

In the present study, a reentrant beam was constructed as shown in the compression tests in Figure 10. A numerical model representing the structure was constructed and validated with experimental data. From this, some simulation was performed with different configurations to understand at which intervals we could find the optimal point, so the length of the oblique bar will vary between 6mm to 10mm , the length of the horizontal bar will vary between 14mm to 18mm, and the angle α ($\alpha = 90 - \theta$) will vary between 50° to 70°. From this interval, you can use a statistical technique called response surface methodology to create a series of experiments. The design of experiments and the experimental results are shown in Table 3. The answers of interest are Poisson's ratio (ν), Failure load (Q_u), Buckling load (λ), Natural frequency (ω_n) and Mass (M).

Table 3 – Design of experiment considering three manufacturing (design) factors.

	Variables			Responses				
Exp.	*α(°)*	*b(mm)*	*l (mm)*	*ν*	Q_U *(N)*	λ (N)	ω_n *(Hz)*	*M(g)*
1	50	14	6	-1,24	19350	101100	342,4	57,42
2	70	14	6	-1,98	18330	110900	332,0	57,42
3	50	18	6	-1,25	17990	133200	320,2	66,42
4	70	18	6	-2,00	16200	129700	294,9	66,42
5	50	14	10	-1,38	7643	32390	125,2	74,70
6	70	14	10	-2,59	7989	44350	146,1	74,70
7	50	18	10	-1,39	9422	37650	132,1	83,70
8	70	18	10	-2,61	8366	45240	137,8	83,70
9	50	16	8	-1,33	13800	58830	202,5	70,56
10	70	16	8	-2,35	9191	67770	204,2	70,56
11	60	14	8	-1,77	12260	60390	204,1	66,06
12	60	18	8	-1,78	12290	62650	193,9	75,06
13	60	16	6	-1,61	17640	104100	356,2	61,92
14	60	16	10	-1,89	8564	39200	134,1	79,20
15	60	16	8	-1,78	12570	62040	199,8	70,56
16	60	16	8	-1,79	12280	60660	195,4	71,22
17	60	16	8	-1,78	12350	60510	195,9	70,77
18	60	16	8	-1,77	12790	63620	203,9	70,35
19	60	16	8	-1,77	12630	62050	199,6	70,78
20	60	16	8	-1,78	12410	60540	195,7	70,99

From the results shown in Table 3 it is possible to find regression models that represent each of the answers of interest. The models are shown in Table 4 and, to verify that these models are reliable, the adjusted R^2 parameter is analyzed, as shown in table 5.

Table 4: Regression coefficients for fit regression model.

Response	X_1	X_2	X_3	X_1^2	X_2^2	X_3^2	X_1X_2	X_1X_3	X_2X_3	C
M		2,25	4,32							0,066
ν	0,0681		0,1385	0,0006		0,0078		0,0059		-2,537
λ	-5297	14153	-48851	47		3264			-1398	343939
ω_n	-3,19	-18,02	-231,2			8,15		0,389	1,809	1589
Q_u	-81,3	-1477	-8769			223,1			176,4	74049

Table 5: Model Summary for fit regression model.

Response	S	R^2 (adj)
M	0,198716	99,92%
ν	0,019170	99,76%
λ	4334,500	97,87%
ω_n	9,363410	98,37%
Q_u	785,6230	95,30%

The Table 5 shows that the adjustment of the data to the models was high, all above 95%, so it can be concluded that the models are representing the data well. Other statistical analyses can be done to verify which factors are important to the model, for example, however this will not be done here, because the focus is to show the process of optimizing an auxetic structure. Thus, the models shown in Table 4 will be used as the objective function of the optimization process and the range of variation of the variables will be the constraints. Equation 36 shows the compression performance optimization design and Figure 16 the Pareto's front for this problem.

$$\begin{aligned} &\min F(\boldsymbol{X})=\{-Q_u, -\lambda, \nu\} \\ &\textit{subject to:} \\ &14 \le b \le 18 \text{ [mm]} \\ &6 \le l \le 10 \text{ [mm]} \\ &50 \le \alpha \le 70 \text{ [°]} \end{aligned} \tag{36}$$

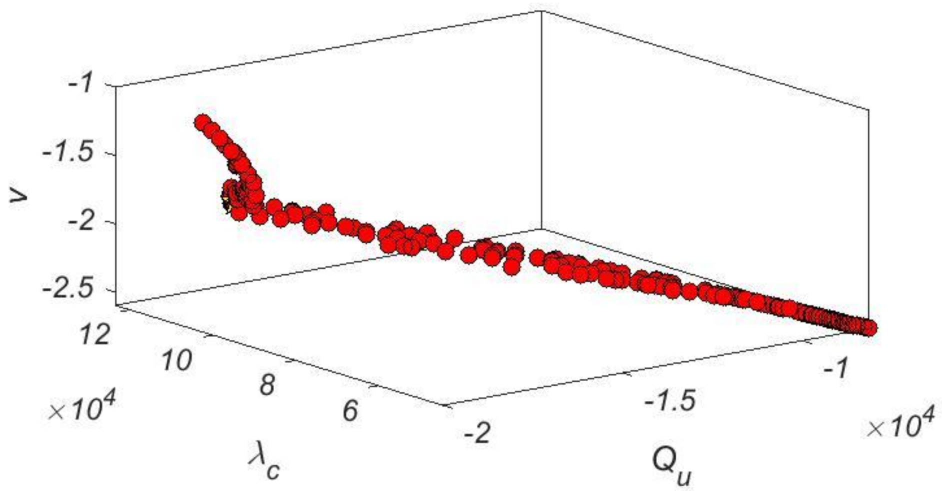

Figure 16: Pareto's front for Poisson's ratio, failure load and critical buckling load of reentrant auxetic beam.

It is perceived by Figure 16 that it is not possible to improve all responses simultaneously, that is, to decrease the Poisson's ratio, both the failure load and the critical buckling load will also decrease. All red dots on the chart are great points and can be chosen. In this work, we used the TOPSIS criterion to decide which point of the chart will be chosen, this criterium choose the point farthest from the worst result and the closest to the best result. The chosen point is shown in Table 6 and Figure 17 shows the optimized structure and the initial structure. The results obtained with this configuration compared to the initial configuration are shown in Table 7.

Table 6 - Optimum configuration for compression performance of reentrant auxetic beam.

Configuration	
θ (°)	70
b (mm)	16
l (mm)	6

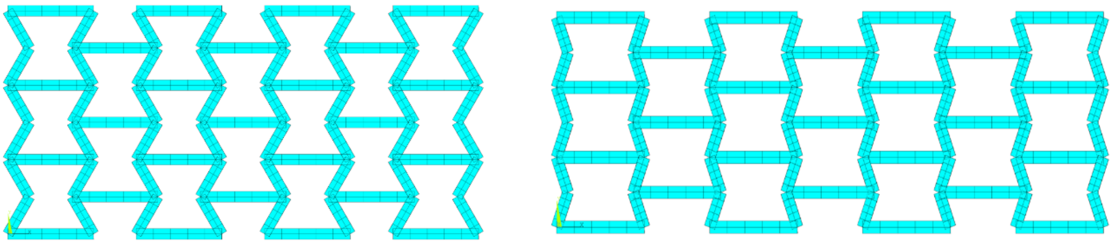

(a) (b)

Figure 17: The (a) Initial and (b) optimized reentrant beam structure.

Table 7: Comparison between the initial and the optimized reentrant beam structure results (compression performance).

Response	Initial structure results	Optimized structure results	Improvement
Q_u (N)	12570	17160	26.75%
λ (N)	62040	108500	42.82%
ν	-1.78	-1.99	10.55%
ω_n (Hz)	199.80	312.88	36.14%
M (g)	70.56	61.92	12.24%

Similarly, the model can be optimized to improve the modal performance of the structure. The goal may be to maximize natural frequency and minimize Poisson's ratio and mass. The minimization in this case is to decrease the mass value and to leave the structure with a more pronounced auxetic behavior. The maximization of the natural frequency aims to remove the frequency of the vibration frequency structure of most mechanical equipment. Thus, optimization can be represented in Equation 37. It is noticed that the restrictions are the intervals defined for each of the variables and Figure 18 shows the Pareto chart for the three responses simultaneously and Table 8 shows the optimal point chosen by the TOPSIS criterion.

$$\begin{aligned} &\min F(\boldsymbol{X})=\{-\omega_n, v, M\} \\ &\textit{subject to:} \\ &14 \leq b \leq 18 \text{ [mm]} \\ &6 \leq l \leq 10 \text{ [mm]} \\ &50 \leq \alpha \leq 70 \text{ [°]} \end{aligned} \tag{37}$$

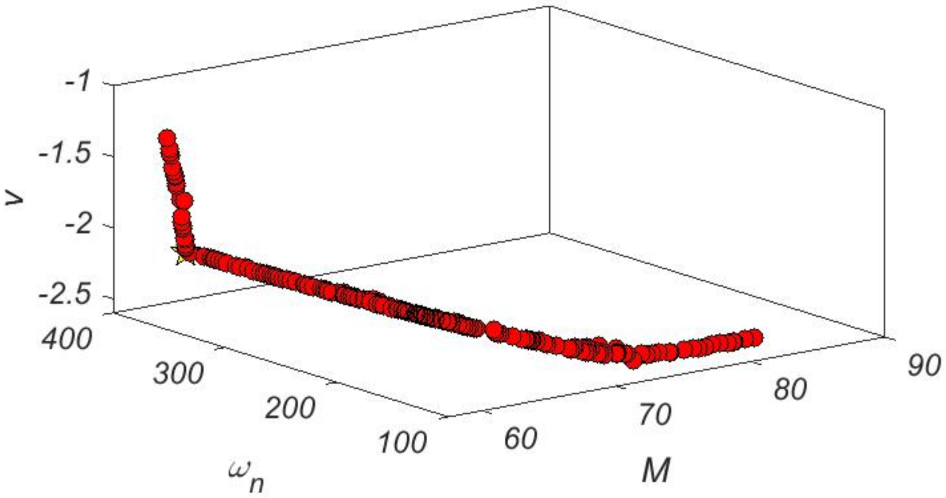

Figure 18: Pareto's front for Poisson ratio, natural frequency, and mass of the reentrant auxetic beam.

Table 8: Optimum configuration for modal performance of reentrant auxetic beam.

Configuration	
θ (°)	70
b (mm)	14
l (mm)	6

It is perceived by figure 18 that it is possible to increase the natural frequency and reduce the mass, as they are inversely proportional parameters. However, this condition implies increasing the Poisson's ratio, as they are conflicting objectives. Thus, by the TOPSIS criterion, the point marked a yellow star was chosen on the chart that corresponds to the point shown in Table 8 and the Table 9 shows the comparison between the initial and the optimized configuration. Figure 19 shows the initial and optimized structure, while the table shows the comparison of the results between the structures.

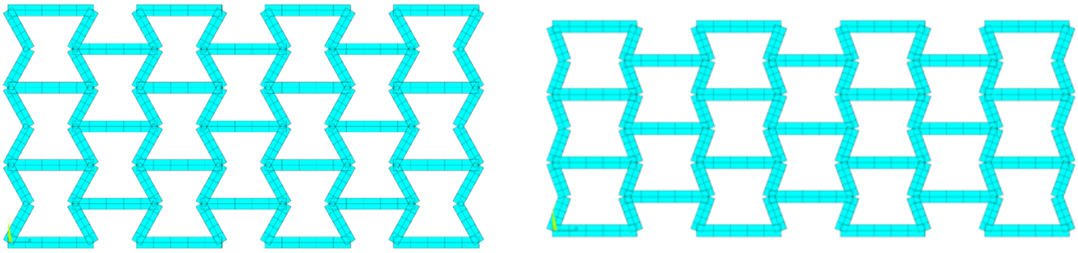

(a) (b)

Figure 19: The model of (a) initial and (b) optimized auxetic beam structure for modal performance.

Table 9: Comparison between the initial and the optimized auxetic beam structure results (Modal performance).

Response	Initial structure results	Optimized structure results	Improvement
Q_u (N)	12570	18330	31.42%
λ (N)	62040	110900	44.06%
ν	-1.78	-1.98	10.10%
ω_n (Hz)	199.80	332.10	39.83%
M (g)	70.56	57.42	18.62%

5 Concluding Remarks

The chapter focused on showing the reader what auxetic structures are. It has been reported that these structures have negative Poisson coefficient and that there are several improved properties because of this characteristic. These structures can be constructed with auxetic or conventional materials, and the configuration adopted is fundamental for this behavior. Some unit cells have been shown and the choice to adopt any of them depends on the application of the structure and manufacturing processes available.

This chapter also showed the manufacture of a reentrant girder through additive manufacturing. This process facilitated the development of new structures with negative Poisson coefficient, because it removed the manufacturing difficulty that exists through conventional processes, such as machining, for example. This structure was submitted to a compression test and the results were shown so that the reader has knowledge of the performance of this structure.

Finally, it proved to be a way to optimize an auxetic model, reaching the optimal parameters of structure construction. The results obtained from the optimal model were compared with the initial model to verify the improvement of the structure. This methodology proved very propitious to perform the parametric optimization of structures with negative Poisson coefficient and the techniques used here can be applied in other structures as well.

Acknowledgements

The authors would like to acknowledge the financial support from the Brazilian agency CNPq (Conselho Nacional de Desenvolvimento Científico e Tecnológico - 431219/2018-4), CAPES (Coordenação de Aperfeiçoamento de Pessoal de Nível Superior), and FAPEMIG (Fundação de Amparo à Pesquisa do Estado de Minas Gerais - APQ-00385-18).

References

Evans, Ken. and Andrew Alderson. 2000. Auxetic materials: Functional materials and structures from lateral thinking. Advanced Materials, 12(9): 617–628.

Ouisse, M., Collet, M., & Scarpa, F. (2016). A piezo-shunted kirigami auxetic lattice for adaptive elastic wave filtering. Smart Materials and Structures, 25(11), 115016.

Vinay, V. C., & Varma, D. M. (2019). Fabrication and testing of auxetic foams for rehabilitation applications. Journal of the Indian Institute of Science, 1-8.

Duncan, O., Shepherd, T., Moroney, C., Foster, L., Venkatraman, P. D., Winwood, K., ... & Alderson, A. (2018). Review of auxetic materials for sports applications: Expanding options in comfort and protection. Applied Sciences, 8(6), 941.

Gatt, Ruben. Luke Mizzi, Joseph Azzopardi, Keith Azzopardi, Daphne Attard, Aaron Casha, Joseph Brifa and Joseph Grima. 2015. Hierarchical Auxetic Mechanical Metamaterials. Sci. Rep. 5, 246(9):2025–2032. https://doi.org/10.1002/pssb.20098203335

Linforth, S. J. (2020). Auxetic Armour System for Protection Against Soil Blast Loading (Doctoral dissertation).

Duncan, O., Foster, L., Senior, T., Alderson, A., & Allen, T. (2016). Quasi-static characterisation and impact testing of auxetic foam for sports safety applications. Smart Materials and Structures, 25(5), 054014.

Tomažinčič, D.; Nečemer, B.; Vesenjak, M.; Klemenc, J. Low-cycle fatigue life of thin-plate auxetic cellular structures made from aluminium alloy 7075-T651. Fatigue Fract. Eng. Mater. Struct. 2019, 42, 1022–1036.

K.E. Evans, K.L. Alderson, Auxetic materials: the positive side of being negative, Eng. Sci. Educ. J. 9 (4) (2000) 148–154.

F. Scarpa, L.G. Ciffo, J.R. Yates, Dynamic properties of high structural integrity auxetic open cell foam, Smart Mater. Struct. 13 (1) (2003) 49.

R.S. Lakes, K. Elms, Indentability of conventional and negative Poisson's ratio foams, J. Compos. Mater. 27 (12) (1993) 1193–1202.

C. Lira, F. Scarpa, R. Rajasekaran, A gradient cellular core for aeroengine fan blades based on auxetic configurations, J. Intell. Mater. Syst. Struct. 22 (9) (2011) 907–917.

L. White, Auxetic foam set for use in smart filters and wound dressings, Urethanes Technol. Int. 26 (4) (2009) 34–36.

Gupta, N., & Gupta, K. M. (2005, March). Metamaterial and auxetic hybrid composite antennas. In antenna technology: small antennas and novel metamaterials, 2005. IWAT 2005. IEEE international workshop on (pp. 414-417). IEEE. 36

C. Yang, H.D. Vora, Y.B. Chang, Evaluation of auxetic polymeric structures for use in protective pads, ASME 2016 International Mechanical Engineering Congress and Exposition, Am. Soc. Mech. Eng., 2016, (pp. V009T12A066-V009T12A066).

Imbalzano, G., Tran, P., Ngo, T. D., & Lee, P. V. (2017). Three-dimensional modelling of auxetic sandwich panels for localised impact resistance. *Journal of Sandwich Structures & Materials*, *19*(3), 291-316.

Wu, W., Hu, W., Qian, G., Liao, H., Xu, X., & Berto, F. (2019). Mechanical design and multifunctional applications of chiral mechanical metamaterials: A review. *Materials & Design*, *180*, 107950.

Mir, M., Ali, M. N., Sami, J., & Ansari, U. (2014). Review of mechanics and applications of auxetic structures. *Advances in Materials Science and Engineering*, *2014*.

Lakes, Roderic. 1987. Foam structures with a negative Poisson's ratio, Science, 235: 1038– 1040.

Zahra, T., & Dhanasekar, M. (2017). Characterisation of cementitious polymer mortar–Auxetic foam composites. Construction and Building Materials, 147, 143-159.

Ren, X., Shen, J. H., Ghaedizadeh, A., Tian, H. Q., & Xie, M. (2016). Numerical simulations of 3D metallic auxetic metamaterials in both compression and tension. In Applied Mechanics and Materials (Vol. 846, pp. 565-570). Trans Tech Publications Ltd.

Li, T., Liu, F., & Wang, L. (2020). Enhancing indentation and impact resistance in auxetic composite materials. Composites Part B: Engineering, 198, 108229.

Hu, J. S., Wang, B. L., Li, J. E., & Wang, K. F. (2020). Thermal shock resistance behavior of auxetic ceramic honeycombs with a central crack or an edge crack. Ceramics International.

Evans, K.E.; Nkansah, M.A.; Hutchinson, I.J.; Rogers, S.C. Molecular network design. Nature 1991, 353, 124.

Voigt, W. Lehrbuch der Kristallphysik; Vieweg+Teubner Verlag: Wiesbaden, 1966;

Lees, C.; Vincent, J.F.V.; Hillerton, J.E. Poisson's ratio in skin. Biomed. Mater. Eng. 1991. 37 [53] Yao, Y. T., Alderson, K. L., & Alderson, A. (2016). Modeling of negative Poisson's ratio (auxetic) crystalline cellulose I β. Cellulose, 23(6), 3429-3448.

Najarian, F., Alipour, R., Rad, M. S., Nejad, A. F., & Razavykia, A. (2018). Multi-objective optimization of converting process of auxetic foam using three different statistical methods. Measurement, 119, 108-116.

MEENA, Kusum; SINGAMNENI, Sarat. Novel hybrid auxetic structures for improved inplane mechanical properties via additive manufacturing. Mechanics of Materials, v. 158, p. 103890, 2021.

Alderson, A., & Evans, K. E. (2001). Rotation and dilation deformation mechanisms for auxetic behaviour in the α-cristobalite tetrahedral framework structure. Physics and Chemistry of Minerals, 28(10), 711-718.

Gao, J., Xue, H., Gao, L., & Luo, Z. (2019). Topology optimization for auxetic metamaterials based on isogeometric analysis. Computer Methods in Applied Mechanics and Engineering, 352, 211-236.

Ren, X., Shen, J., Tran, P., Ngo, T.D., Xie, Y.M., 2018. Design and characterisation of a tunable 3D buckling-induced auxetic metamaterial. Mater. Des. 139, 336 – 342.

Liu, W., Wang, N., Luo, T., Lin, Z., 2016. In-plane dynamic crushing of re-entrant auxetic cellular structure. Mater. Des. 100, 84–91.

Wang, X., Wang, B., Wen, Z., Ma, L., 2018. Fabrication and mechanical properties of CFRP composite three-dimensional double-arrow-head auxetic structure. Compos. Sci. Tech., 164, 92- 102.

Zhang, H., Luo, Y., Kang, Z., 2018. Bi-material microstructural design of chiral auxetic metamaterials using topology optimization. Compos. Struct. 195, 232-248.

Grima, J.N., Missi, L., Azzopardi, K.M., Gatt, R., 2016. Auxetic perforated mechanical metamaterials with randomly oriented cuts. Adv. Mater. 28, 385-389.

JOHNSTON, Ross; KAZANCI, Zafer. Analysis of additively manufactured (3D printed) dualmaterial auxetic structures under compression. Additive Manufacturing, v. 38, p. 101783, 2021.

Gibson, L.J., The mechanics of two-dimensional cellular material, proceedings of the royal Society of London series A – mathematical physical and engineering Science 382:25 (1982)

Larsen, U. D., Signund, O., & Bouwsta, S. (1997). Design and fabrication of compliant micromechanisms and structures with negative Poisson's ratio. *Journal of microelectromechanical systems*, *6*(2), 99-106.

Qiao, J. X., & Chen, C. Q. (2015). Impact resistance of uniform and functionally graded auxetic double arrowhead honeycombs. *International Journal of Impact Engineering*, *83*, 47-58.

J.N. Grima, K.E. Evans, Auxetic behavior from rotating squares, J. Mater. Sci. Lett. 19 (2000) 1563–1565, https://doi.org/10.1023/A:1006781224002.

Grima JN, Zammit V, Gatt R, Alderson A, Evans KE (2007) Auxetic behavior from rotating semirigid units. Phys Status Solidi B 244(3):866–882

Nečemer, B., Glodež, S., Novak, N., & Kramberger, J. (2020). Numerical modelling of a chiral auxetic cellular structure under multiaxial loading conditions. Theoretical and Applied Fracture Mechanics, 107, 102514

D. Prall, R. Lakes, Properties of a chiral honeycomb with a Poisson’s ratio of –1, Int. J. Mech. Sci. 39 (1997) 305–314, https://doi.org/10.1016/j.jpeds.2009.04.058.

Foster, L., Peketi, P., Allen, T., Senior, T., Duncan, O., & Alderson, A. (2018). Application of auxetic foam in sports helmets. Applied Sciences, 8(3), 354.

Shah, I. A., Khan, R., Koloor, S. S. R., Petrů, M., Badshah, S., Ahmad, S., & Amjad, M. (2022). Finite Element Analysis of the Ballistic Impact on Auxetic Sandwich Composite Human Body Armor. *Materials*, *15*(6), 2064.

Shepherd, T., Winwood, K., Venkatraman, P., Alderson, A., & Allen, T. (2020). Validation of a Finite Element Modeling Process for Auxetic Structures under Impact. physica status solidi (b), 1900197.

Wang, Y., Zhao, W., Zhou, G., Gao, Q., & Wang, C. (2018). Optimization of an auxetic jounce bumper based on Gaussian process metamodel and series hybrid GA-SQP algorithm. *Structural and Multidisciplinary Optimization*, *57*(6), 2515-2525.

Zhou, G., Ma, Z. D., Li, G., Cheng, A., Duan, L., & Zhao, W. (2016). Design optimization of a novel NPR crash box based on multi-objective genetic algorithm. *Structural and Multidisciplinary Optimization*, *54*(3), 673-684.

Gao, Q., Zhao, X., Wang, C., Wang, L., & Ma, Z. (2018). Multi-objective crashworthiness optimization for an auxetic cylindrical structure under axial impact loading. *Materials & design*, *143*, 120-130.

Lee, W., Jeong, Y., Yoo, J., Huh, H., Park, S. J., Park, S. H., & Yoon, J. (2019). Effect of auxetic structures on crash behavior of cylindrical tube. *Composite Structures*, *208*, 836-846.

Budarapu, P. R., YB, S. S., & Natarajan, R. (2016). Design concepts of an aircraft wing: composite and morphing airfoil with auxetic structures. *Frontiers of Structural and Civil Engineering*, *10*(4), 394-408.

Francisco, M. B., Pereira, J. L. J., Oliver, G. A., Roque da Silva, L. R., Cunha Jr, S. S., & Gomes, G. F. (2021). A review on the energy absorption response and structural applications of auxetic structures. *Mechanics of Advanced Materials and Structures*, 1-20.

Wang, T., An, J., He, H., Wen, X., & Xi, X. (2021). A novel 3D impact energy absorption structure with negative Poisson's ratio and its application in aircraft crashworthiness. *Composite Structures*, *262*, 113663.

Günaydın, K., Eren, Z., Kazancı, Z., Scarpa, F., Grande, A. M., & Türkmen, H. S. (2019). In-plane compression behavior of anti-tetrachiral and re-entrant lattices. *Smart Materials and Structures*, *28*(11), 115028.

Lee, W., Jeong, Y., Yoo, J., Huh, H., Park, S. J., Park, S. H., & Yoon, J. (2019). Effect of auxetic structures on crash behavior of cylindrical tube. *Composite Structures*, *208*, 836-846.

Qi, C., Remennikov, A., Pei, L. Z., Yang, S., Yu, Z. H., & Ngo, T. D. (2017). Impact and close-in blast response of auxetic honeycomb-cored sandwich panels: experimental tests and numerical simulations. *Composite structures*, *180*, 161-178.

Al-Rifaie, H., & Sumelka, W. (2019). The development of a new shock absorbing Uniaxial Graded Auxetic Damper (UGAD). *Materials*, *12*(16), 2573.